New Phytologist

Research

Heterogeneous distribution of pectin epitopes and calcium in different pit types of four angiosperm species

Lenka Plavcová and Uwe G. Hacke

Department of Renewable Resources, University of Alberta, 442 Earth Sciences Building, Edmonton, AB, Canada, T6G 2E3

Author for correspondence:
Uwe G. Hacke
Tel: +1 780 492 8511
Email: uwe.hacke@ualberta.ca

Received: *25 May 2011*
Accepted: *29 June 2011*

New Phytologist (2011) **192**: 885–897
doi: 10.1111/j.1469-8137.2011.03842.x

Key words: calcium, cavitation, electron microcopy, pectin, pit membrane, ray parenchyma, vessel, xylem.

Summary

• Intervessel pits act as safety valves that prevent the spread of xylem embolism. Pectin–calcium crosslinks within the pit membrane have been proposed to affect xylem vulnerability to cavitation. However, as the chemical composition of pit membranes is poorly understood, this hypothesis has not been verified.

• Using electron microscopy, immunolabeling, an antimonate precipitation technique, and ruthenium red staining, we studied the distribution of selected polysaccharides and calcium in the pit membranes of four angiosperm tree species. We tested whether shifts in xylem vulnerability resulting from perfusion of stems with a calcium chelating agent corresponded with the distribution of pectic homogalacturonans (HG) and/or calcium within interconduit pit membranes.

• No HG were detected in the main part of intervessel pit membranes, but were consistently found in the marginal membrane region known as the annulus. Calcium colocalized with HG in the annulus. In contrast to intervessel pits, the membrane of vessel-ray pits showed a high pectin content.

• The presence of two distinct chemical domains, the annulus and the actual pit membrane, can have substantial implications for pit membrane functioning. We propose that the annulus could affect the observed shift in xylem vulnerability after calcium removal by allowing increased pit membrane deflection.

Introduction

Water and nutrients move through a complex network of xylem conduits that, when mature, are dead and void of cellular content. Water movement is driven by a gradient in negative pressure that is a result of evaporation from the tiny menisci localized in the cell walls of leaf parenchyma. Consequently, xylem sap is in a metastable state and hydraulic failure can readily occur (Tyree & Zimmermann, 2002). As the xylem pressure decreases owing to increased evaporative demand or lack of soil moisture, there is a higher risk of water columns essentially 'breaking' and xylem conduits becoming air-filled (i.e. embolized). Embolized conduits are temporarily or permanently disconnected from the transpiration stream and hydraulic conductivity (k_h) decreases.

Interconduit pits connect adjacent conduits to permit water flow while preventing the spread of air from embolized conduits to adjacent functional ones (Sperry & Tyree, 1988; Sperry & Hacke, 2004; Choat *et al.*, 2008). According to the air-seeding hypothesis, microporous pit membranes will support an air–-water interface until the pressure difference across the membrane overcomes the capillary forces (Sperry *et al.*, 1996). The air-seeding threshold is inversely related to the pore diameter, such that higher pit membrane porosity will result in more vulnerable xylem (Jarbeau *et al.*, 1995; Choat *et al.*, 2008). A consequence of the role of interconduit pits as safety valves is that they provide a significant constraint to water flow. In both conifer tracheids and angiosperm vessels, interconduit pits contributed, on average, more than half of the total conduit resistivity (Pittermann *et al.*, 2005; Hacke *et al.*, 2006).

Pits are also found between (axial and ray) parenchyma cells and xylem conduits, thus providing an interface between the living and dead components of the xylem. Controlled fluxes of various solutes including ions (De Boer & Volkov, 2003; Nardini *et al.*, 2010), sugars (Sauter *et al.*, 1973; Salleo *et al.*, 2009) and amino acids (Sauter & Van Cleve, 1992) occur between ray cells and vessels. These exchange processes are most likely influenced by the properties of vessel-ray pit membranes. In addition, vessel-ray pits may play a role in embolism refilling as water appears to

enter refilling vessels through this interface (Braun, 1970; Brodersen *et al.*, 2010).

The permeability of pit membranes in both intervessel and vessel-ray pits is critical for their function. The porosity and permeability of pit membranes are likely to be affected by the chemical composition of the membrane. However, our knowledge of pit membrane chemistry is limited. Pit membranes develop from the compound middle lamella (cml) (Evert, 2006), and it is usually assumed that their chemical composition resembles that of a typical primary cell wall. However, this assumption awaits further testing because of the extensive remodeling and hydrolysis of the original primary wall that takes place during pit membrane differentiation (Schmid & Machado, 1968; O'Brien, 1970; Morrow & Dute, 1998). According to the current paradigm, pit membranes are composed of multiple layers of cellulose microfibrils embedded in a matrix of hemicellulose and pectins (Choat *et al.*, 2008). Structural proteins that are common in the primary cell wall (Cassab, 1998; Valentin *et al.*, 2010) may also occur in pit membranes (Harrak *et al.*, 1999).

Experimental evidence suggests that pectins play important roles in pit membrane functioning (Wisniewski *et al.*, 1991; Zwieniecki *et al.*, 2001; Boyce *et al.*, 2004; van Ieperen, 2007; Cochard *et al.*, 2010; Nardini *et al.*, 2010). Pectins are a highly complex and heterogeneous group of polysaccharides rich in galacturonic acid (GalA). Different domains of pectins can be distinguished based on their biochemical properties; namely homogalacturonan (HG), rhamnogalacturonan-I (RG-I) and rhamnogalacturonan-II (Willats *et al.*, 2001). Homogalacturonans are linear polymers of 1,4-linked α-D-GalA and are the most abundant pectic domain in the primary cell wall comprising up to 60% of total pectin (O'Neill & William, 2003). The pectic polymers extensively interact with each other as well as with the other cell wall components (Ryden *et al.*, 2000; MacDougall *et al.*, 2001a; Valentin *et al.*, 2010), but the complexity of these connections is not fully understood.

Because of the presence of numerous carboxyl groups, pectins exhibit properties of polyelectrolytes and have an overall negative charge (Valentin *et al.*, 2010). Calcium pectin gels tend to swell when there is an imbalance in the distribution of mobile counterions between the gel and surrounding solution, which results from the Donnan effect (MacDougall *et al.*, 2001a). Crosslinking of the polymer network constrains the swelling tendencies (MacDougall *et al.*, 2001a). The hydrogel behavior of pectins has been used to explain why the k_h of stem segments is higher when measured with salt solution (typically 10–100 mM KCl solution) compared with perfusion with distilled water (Zwieniecki *et al.*, 2001; Lopez-Portillo *et al.*, 2005; Gasco *et al.*, 2006; van Ieperen, 2007).

In addition to the ionic effect, calcium-mediated crosslinks between pectins have been proposed to influence the vulnerability of xylem to embolism (Sperry & Tyree, 1988). Perfusion of stems with oxalic acid and calcium solution induced greater vulnerability in sugar maple, perhaps by disrupting calcium-mediated crosslinks in the pectins of the pit membrane, which could make the membrane more flexible and allow for transient pore widening (Sperry & Tyree, 1988). Herbette & Cochard (2010) also found that embolism vulnerability increased after perfusing stems with calcium chelating solution. In the presence of > 10 consecutive unmethyl-esterified GalA residues, calcium may interact with the negative charges of the GalA residues to form stable gels based on the 'egg-box' model (Caffall & Mohnen, 2009). While other linkages exist in the pectin network, calcium crosslinking of HG is known to contribute to wall strength (MacDougall *et al.*, 2001a; Micheli, 2001; Caffall & Mohnen, 2009). The presence of low methyl-esterified HG in intervessel pit membranes may therefore be associated with shifts in vulnerability to embolism and may even explain differences in vulnerability between various species (Herbette & Cochard, 2010).

Both the ionic effect and the magnitude of the shift in vulnerability vary greatly among species (Cochard *et al.*, 2010; Herbette & Cochard, 2010; Jansen *et al.*, 2011). While the factors influencing the ionic effect have been previously investigated (Gortan *et al.*, 2011; Jansen *et al.*, 2011), the factors affecting the magnitude of the vulnerability shift after calcium removal are poorly understood. Herbette & Cochard (2010) noted that the shift was greater in more embolism-resistant species. Of the 13 species tested in their study, two (*Salix alba* and *Betula pendula*) remained unaffected by the treatments. It seems possible that pectins were not present in the intervessel pit membranes of these species. Alternatively, if pectins were present, they may not have been capable of forming calcium mediated crosslinks, possibly because of a high degree of esterification. The fact that monoclonal antibodies did not recognize HG in intervessel pit membranes of hybrid poplar saplings (Plavcová *et al.*, 2011) supports the hypothesis that some highly vulnerable species do not possess pectinaceous intervessel pit membranes. The absence of HG would also prevent an increase in vulnerability after calcium removal. To test this hypothesis, we measured the shift in vulnerability in two relatively vulnerable species, *Betula papyrifera* and *Populus balsamifera*, and two more resistant species, *Prunus virginiana* and *Amelanchier alnifolia*. We hypothesized that HG will be absent in the intervessel pit membranes of the two vulnerable species, and that the vulnerability of these species will therefore remain unaffected by calcium removal. We expected the opposite pattern in the two resistant species.

One of the most powerful ways to study pectin in its physiological context is by using anti-pectin antibody probes (Wisniewski & Davis, 1995; Willats *et al.*, 2001). However, this tool has rarely been used on intervessel pit

membranes of woody angiosperms. In this present study, we used immunogold labeling with monoclonal antibodies raised against primary cell wall polysaccharides (HG, RG-I and xyloglucan) to probe the chemical composition of pit membranes. We wished to determine whether the pattern of HG labeling corresponded with the presence of calcium in pit membranes. To do this, we used an antimonate precipitation technique and compared the distribution of HG and calcium at the transmission electron microscopy level. Our final objective was to compare the structure and chemistry of different pit types. Although intervessel and vessel-ray pits may occur in the same vessel element, they have very different functions and may therefore differ in their chemical composition.

Materials and Methods

Plant material

Branches (approx. 1 cm in diameter) of *B. papyrifera* Marsh., *P. balsamifera* L., *P. virginiana* L., and *A. alnifolia* Nutt. were collected in the vicinity of the University of Alberta campus in Edmonton (53°50′ N 113°52′ W). These species were selected to cover a wide range of xylem vulnerability. The trees used for sampling were mature individuals growing in a river valley. For the measurements of vulnerability to embolism, branches were sampled from different randomly selected individuals. The plant material was used immediately or wrapped in plastic bags with wet paper towels and stored at 4°C for no longer than 3 d before the measurements were carried out. For electron microscopy work, xylem samples were collected from the same trees used for the hydraulic measurements. In this case, samples were processed immediately. Samples for hydraulic measurements and transmission electron microscopy (TEM) immunolabeling were collected in October and November 2010, samples for scanning electron microscopy (SEM) observations and TEM calcium localization were collected in February 2011 and samples for ruthenium red staining were taken in May 2011. In addition, a limited set of hydraulic measurements was carried out in February to verify that vulnerability to embolism did not undergo seasonal shifts.

Shifts in vulnerability to embolism

To evaluate the effect of calcium removal on vulnerability to embolism, vulnerability curves were obtained for control stems and stems perfused with a calcium chelating sodium phosphate solution (Herbette & Cochard, 2010). Stem segments were trimmed under water to a length of 14.2 cm. Segments were flushed with the treatment (pH 10) or control (pH 4) 10 mM $NaPO_4$ solution for 30–40 min at 20 kPa. At least 5 ml of solution were perfused through each stem. At pH 10, the phosphate occurs mainly in the form of HPO_4^{2-} anions that readily precipitate Ca^{2+} cations. By contrast, at pH 4 the predominant ionic form of phosphate is $H_2PO_4^-$, which does not bind calcium. The same solutions used for flushing were used during the k_h measurements. After flushing, stem segments were fitted to a tubing apparatus and the maximal hydraulic conductivity (k_{max}) was measured as the flow rate per pressure gradient (Plavcová *et al.*, 2011). The standard centrifuge method (Alder *et al.*, 1997; Li *et al.*, 2008) was used to generate vulnerability curves. Curves were constructed by plotting the negative xylem pressure against the per cent loss of conductivity as described previously (Plavcová *et al.*, 2011). Curves were fitted with a Weibull function and the xylem pressure corresponding to 50% loss of conductivity (P_{50}) was calculated for each stem segment. Six stems per species were measured for each $NaPO_4$ solution.

Scanning electron microscopy

Scanning electron microcopy was used to evaluate whether perfusion with the calcium chelating solution caused changes in pit membrane structure. To prepare the samples for SEM observation, stem segments 5 cm long were perfused with the treatment (pH 10) or control (pH 4) $NaPO_4$ solution at a pressure of 20 kPa for 1 h. Samples were then soaked in the same solution for 24 h at room temperature. Subsequently, segments were rinsed with distilled water and dehydrated through a gradual ethanol series 30–50–70–90% (30 min each) and placed in 100% ethanol overnight. Finally, segments were air-dried for 24 h, split with a razor blade and mounted on aluminum stubs using conductive silver paste. Samples were sputter-coated with chromium and carbon and observed with a field-emission scanning electron microscope (6301F, JOEL, Tokyo, Japan) using 2 kV acceleration voltage. Four different stems of *P. balsamifera* were observed for each $NaPO_4$ solution (pH 4 and 10, respectively). *P. balsamifera* was selected for these SEM observations, because both intervessel and vessel-ray pits were relatively easy to find on a tangential surface plane in comparison with the other three species studied. A semiquantitative elemental analysis via SEM coupled X-ray spectrometry (Princeton Gamma-Tech Inc., Princeton, NJ, USA) was used to assess the chemical composition of conspicuous particles that were abundant in the specimens treated with $NaPO_4$ at pH 10. An acceleration voltage of 50 kV was used for this analysis.

Polysaccharide localization with transmission electron microcopy

For immunolabeling, 1 mm^3 blocks of xylem tissue sampled from the outer part of the stems were fixed in a mixture of 0.2% glutaraldehyde and 3.7% paraformaldehyde in 25 mM piperazine-*N*,*N*′-bis(2-ethanesulfonic acid) (PIPES) for 4.5 h at room temperature. Specimens were

then buffer washed, dehydrated and embedded in LR White resin (London Resin Co., London, UK). Our embedding procedure closely followed the steps previously described by Chaffey (2002), with the modification that we used heat polymerization at 60°C for 24 h. Ultrathin sections (70–90 nm) were cut using an ultramicrotome (Ultracut E, Reichert-Jung, Vienna, Austria) equipped with a diamond knife. Sections were collected on pioloform-coated nickel grids and immunolabeled. Four monoclonal antibodies (JIM5, JIM7, LM6 and LM15; PlantProbes, Leeds, UK) raised against different cell wall polysaccharide epitopes were used in this study. JIM5 and JIM7 bind to HG with a low and a high degree of methyl-esterification, respectively (Knox *et al.*, 1990; Willats *et al.*, 2001; Guillemin *et al.*, 2005). LM6 recognizes arabinan side-chains of RG-I (Ermel *et al.*, 2000; Willats *et al.*, 2001; Guillemin *et al.*, 2005). LM15 is targeted to the XXXG motif of xyloglucan (Marcus *et al.*, 2008). Immunolabeling was performed by floating the grids on drops of successively changing solutions. Sections were preincubated for 10 min on a drop of 0.05 M Tris-buffered saline (pH 7.6) with 0.1% Tween 20 and 0.1% BSA, blocked for 20 min with goat serum (Sigma-Aldrich) diluted 1 : 30 (v : v) in the same buffer, treated with the primary antibody (JIM5, JIM7 and LM6 diluted 1 : 4, LM15 diluted 1 : 3) overnight at 4°C, buffer-washed four times and stained with a secondary antibody, goat-anti rat IgG conjugated with 10 nm gold particles (Sigma-Aldrich) for 1 h. The grids were then extensively washed with buffer and filtered water and finally contrasted with 4% uranyl acetate for 25 min and with Reynolds' lead citrate for 2 min (Reynolds, 1963). Sections were examined under a transmission electron microscope (Morgagni 268; Fei Company, Hillsboro, OR, USA).

The immunolabeling experiment was conceived as a qualitative study aiming to describe the pit membrane chemical composition as well as differences between species. Given our interest in the occurrence of HG in pit membranes, we assessed the labeling density of JIM5 and JIM7 antibodies in the pit membrane annulus. We counted the gold particles in this region. The labeling density in pit membrane annuli was estimated based on 6–15 pits per species and antibody. In addition, the length of the annulus was measured as the distance from the edge of the pit (following the plane of the cml) to the area where the annulus transitioned into the main portion of the pit membrane. This transition zone could be clearly identified based on the difference in the electron density of the membrane. In addition to these measurements, pit membrane diameter was calculated from the pit area assessed in tangential sections with a light microscope at 1000× magnification assuming a circular shape of pit membranes.

To verify the immunolocalization pattern, a histological detection of pectins was performed via ruthenium red staining based on methods described previously (Micheli *et al.*, 2002; Gortan *et al.*, 2011). Xylem tissue was fixed in Karnovsky's fixative containing 0.1% (w : v) ruthenium red for 1.5 h and post-fixated in 1% buffered osmium tetraoxide with 0.1% ruthenium red for 1.5 h at room temperature. Subsequently, samples were dehydrated and embedded in Spurr's resin (EMS, Hatfield, PA, USA). As osmium tetraoxide post-fixation provides some contrast to the tissue, control samples were prepared using the same solutions without ruthenium red. Sections were mounted on coated copper grids and examined without further staining.

Calcium localization

Calcium was localized within the wood tissue using an antimonate precipitation technique (Wick & Hepler, 1980; Slocum & Roux, 1982). This method has been successfully used to localize cell wall-bound calcium in the cambial zone of poplar (Baier *et al.*, 1994; Guglielmino *et al.*, 1997) and European ash (Funada & Catesson, 1991). In this study, small blocks (1 mm^3) of mature xylem were fixed in a mixture of 2% glutaraldehyde, 2.5% formaldehyde, 0.1% tannic acid and 2% potassium antimonate in 0.1 M potassium phosphate buffer at pH 7.6 for 6 h at room temperature in the dark. Specimens were then washed twice for 15 min in antimonate buffer (2% $KSb(OH)_6$ in 0.1 M potassium phosphate at pH 8), postfixed in 1% OsO_4 in antimonate buffer for 2 h, washed three times in antimonate buffer for 10 min, washed for 30 min in 0.01 M potassium phosphate buffer without antimonate at pH 7.6, and finally gradually dehydrated and embedded in Spurr's resin. Ultrathin sections were collected on coated copper grids and observed without further staining.

Statistical analysis

The statistical environment R (R Development Core Team, 2009) was used to perform the statistical analysis. Analysis of variance followed by Tukey's HSD *post hoc* comparison test was conducted to evaluate differences among the species and perfusion solutions. For all tests, differences were considered statistically significant at $P \leq 0.05$.

Results

Shifts in xylem vulnerability to embolism

Vulnerability to embolism was significantly higher in stems perfused with $NaPO_4$ solution at pH 10 compared with the same solution at pH 4 in three out of four species studied ($P < 0.001$) (Fig. 1). The P_{50} values at pH 4 did not differ from values previously measured in our laboratory for these species using a regular measuring solution (20 mM KCl and 1 mM $CaCl_2$) instead of $NaPO_4$ (data not shown). Therefore, perfusion with $NaPO_4$ at pH 4 does not affect xylem vulnerability and the P_{50} at pH 4 reflects the 'native'

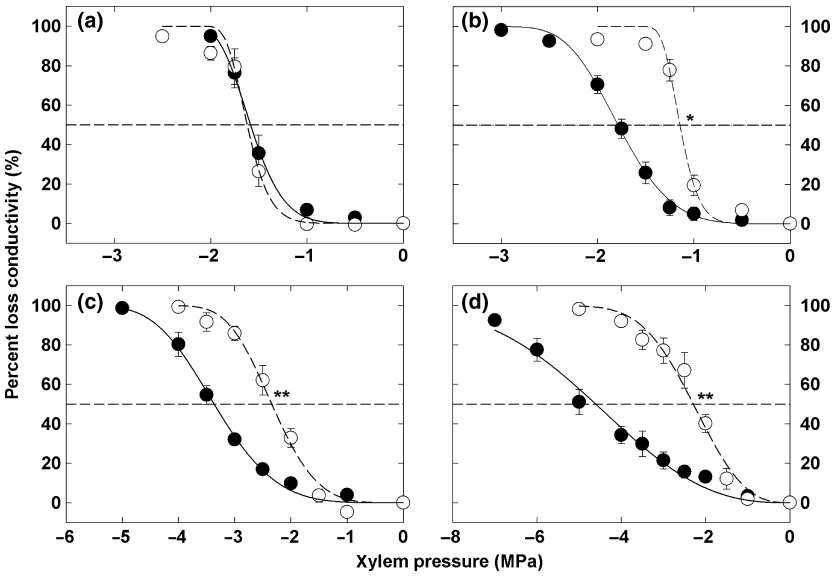

Fig. 1 The effect of calcium removal on xylem vulnerability to embolism. Vulnerability curves of *Betula papyrifera* (a), *Populus balsamifera* (b), *Prunus virginiana* (c) and *Amelanchier alnifolia* (d) in stems perfused with sodium phosphate solution at pH 10 (open circles) or pH 4 (closed circles). The phosphate solution at pH 10 is capable of chelating calcium, while the solution at pH 4 is a nonchelating control. Error bars show standard error of mean (n = 6). * and ** indicate that the xylem pressure at which stems showed 50% loss of conductivity (P_{50}) differed ($P < 0.05$ and $P < 0.001$, respectively) between stems perfused with treatment vs control phosphate solution (Tukey HSD test).

xylem vulnerability. The difference in P_{50} (ΔP_{50}) in stems infiltrated with solutions of different pH was largest in the most resistant species, *A. alnifolia* (ΔP_{50} = 2.12 ± 0.16 MPa). The magnitude of the shift in P_{50} was proportional to the native vulnerability of species, with more resistant species shifting more (see the Supporting Information, Fig. S1). Although their P_{50} values at pH 4 did not differ (P = 0.945), *P. balsamifera* exhibited a significant shift in vulnerability (P = 0.020) while *B. papyrifera* did not (P = 0.998). The correlation between ΔP_{50} and the P_{50} at pH 4 closely followed the relationship observed by Herbette & Cochard (2010) although we used different species and a different centrifuge method to measure the vulnerability curves.

Scanning electron microcopy

Scanning electron microscopy was used to test if perfusion with calcium chelating solution caused visible changes in pit membrane structure. Spherical particles were often found in the vessel lumens of samples treated with $NaPO_4$ at pH 10, but were rare in samples treated with $NaPO_4$ solution at pH 4 (Fig. 2). Semiquantitative elemental analysis with an X-ray analysis system coupled with the SEM microscope revealed that the particles were rich in phosphorus, calcium, sodium and magnesium. At pH 10, but not at pH 4, these particles were consistently found in high concentrations on the surface of vessel-ray pit membranes (Fig. 2b). At pH 10, precipitate was occasionally found on the surface of intervesssel pit membranes (images not shown). However, compared with vessel-ray pit membranes, intervessel pit membranes had far fewer particles, and precipitate was only sporadically observed in different samples. The distribution of these particles within the intervessel pit membrane seemed fairly random. However, in several instances more particles were found around the periphery of the pit membrane, that is, the annulus region.

Distribution of high and low methyl-esterified homogalacturonan

None of the antibodies used in this study showed a strong signal in the entire pit membrane of interconduit pits.

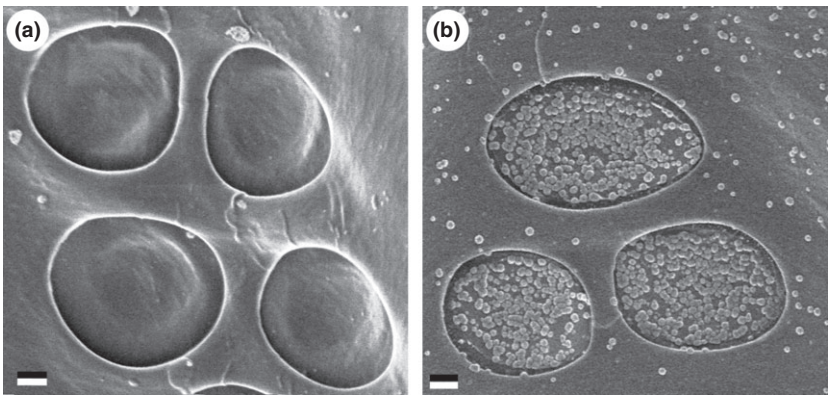

Fig. 2 Scanning electron micrographs of vessel-ray pits in stems of *Populus balsamifera* perfused with sodium phosphate solution at pH 4 (a) or pH 10 (b). Pit membranes are viewed from the vessel lumen through wide apertures in the secondary cell wall. Conspicuous spherical particles were often found in the vessel lumen of samples perfused with the solution at pH 10 and were especially abundant on the surface of vessel-ray pit membranes. These particles were rich in phosphorus, calcium, magnesium and sodium, as revealed with a semiquantitative elemental analysis. Bars, 1 μm.

Nevertheless, several labeling patterns could be distinguished (Table 1). JIM7 labeling was more or less evenly distributed in the cml (Fig. 3a). By contrast, the JIM5 epitope was only rarely found in the cml between two cells, but was more frequently present in the cml of cell corners. This pattern indicates that the HG in the cml was largely esterified. Pit membranes of all species showed a distinct annulus, that is, an electron-dense area near the periphery of the pit membrane. The annulus was substantially shorter in *B. papyrifera* in comparison with the other species (Table 2). Importantly, this region was strongly labeled with both JIM5 and JIM7 (Fig. 3a,b,c). Whereas JIM7 labeling was usually evident throughout the entire annulus region (Fig. 3a), the JIM5 epitope was often confined to the tip of the annulus (Fig. 3b,c). The number of gold particles per annulus for JIM5 and JIM7 varied, on average, from 5 to 15 between the species (Table 2). These counts provide an estimate of the ratio between low and high methyl-esterified HG in the annulus. This ratio was highest in *B. papyrifera*.

The pit annuli of imperforate tracheary elements in *P. virginiana*, *A. alnifolia* and *B. papyrifera* showed the same HG labeling pattern that was observed in intervessel pits (Fig. 4a). We use the term 'imperforate tracheary element' in the all-inclusive sense outlined by Carlquist (1986). Pits of imperforate tracheary elements in *P. virginiana* and *A. alnifolia* were distinct in that they often had pseudotori thickenings. The attachment of the cap-like thickenings to the membrane varied. Sometimes

Table 1 The intensity and localization of immunogold labeling for polysaccharide-specific antibodies JIM5, JIM7, LM6 and LM15

Antibody	JIM5	JIM7	LM6	LM15
Epitope	Low methyl-esterified/nonesterified HG	Methyl-esterified HG	(1-5)-α-l-arabinan of RG-I	XXXG motif of XG
Intervessel pit membrane	–	–	–/+	–/+
Annulus	++	++	–/+	–/+
Vessel-ray pit membrane	++	++	+	–/+
Amorphous layer of ray cells	++	++	++	–/+
cml-between two cells	–/+	+	+	+
cml-cell corners	+	+	+	+
Pseudotori	–	–/+	++	–
Membrane under pseudotorus	++	++	–/+	–

++, strong signal/enrichment in labeling; +, weak signal; –, no signal; cml, compound middle lamella; HG, homogalacturonan; RG-I, rhamnogalacturonan I; XG, xyloglucan.

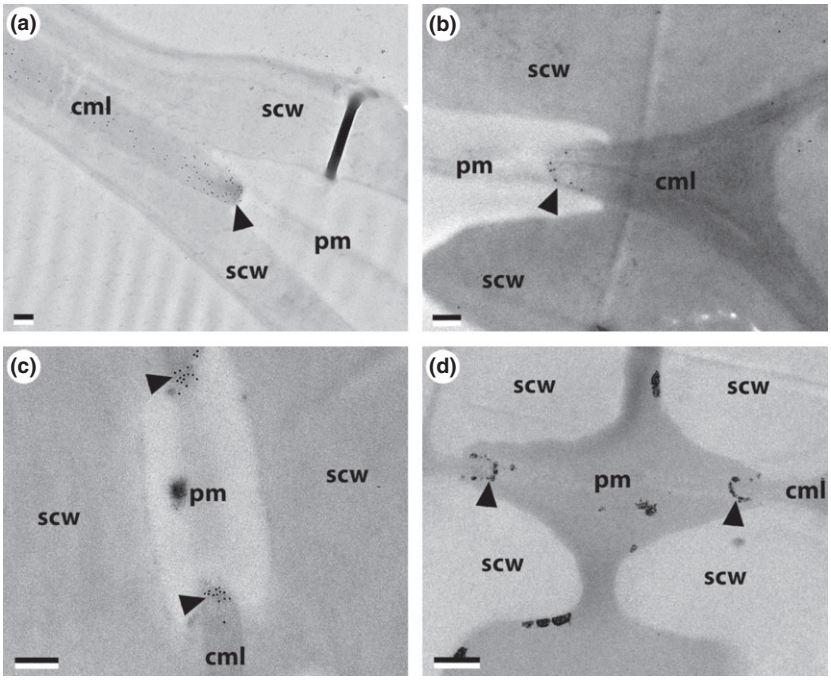

Fig. 3 Transmission electron micrographs of the pit membrane annulus region showing the distribution of homogalacturonan (HG) (a,b,c) and calcium precipitate (d) as revealed by immunogold labeling (a,b,c) and an antimonate precipitation technique (d). Labeling with JIM7 antibody is indicative of high methyl-esterified HG and was evident throughout the entire annulus region (a). Labeling with JIM5 antibody shows the distribution of low methyl-esterified HG and was often restricted to the tip of the annulus (b,c). Electron-dense calcium precipitates in the annulus (d) closely resembled the JIM5 labeling pattern (compare b and d). Micrographs show pits of *Populus balsamifera* labeled with JIM7 (a), *Prunus virginiana* labeled with JIM5 (b), *Betula papyrifera* labeled with JIM5 (c) and *Amelanchier alnifolia* after antimonate precipitation (d). Arrow heads point to annuli; cml, compound middle lamella; pm, pit membrane; scw, secondary cell wall. Bars, (a–c) 0.2 μm, (d) 0.5 μm.

the pads were closely attached to the membrane. In those cases, strong labeling with JIM7 was found throughout the inner membrane layer, that is the part of the membrane located between the pads (images not shown). In other cases, the thickenings were somewhat disconnected and formed hollow horseshoe- or cap-like structures that overarched the membrane (Fig. 4a). Strong labeling with both JIM5 and JIM7 was seen on the inner surface of the cap-like thickenings (Fig. 4a, arrows).

In contrast to intervessel pit membranes, the membranes of vessel-ray pits consistently exhibited strong labeling for both JIM5 and JIM7 (Fig. 4c). JIM5 was localized closer to the surface of the membrane facing the vessel lumen (Fig. 4c), whereas the density of JIM7 labeling was more homogeneous across the pit membrane. JIM5 and JIM7 labeling was also detected in the amorphous cell wall layer of ray parenchyma cells. In *A. alnifolia*, JIM5 labeling was enriched in a darker band that traversed the amorphous layer (Fig. 4c).

The HG distribution patterns, as detected with antibodies, were verified using ruthenium red staining. Electron-dense regions indicated a positive staining reaction with ruthenium red. In agreement with the immunolabeling results, staining was consistently observed in the annulus of intervessel pits (Fig. 5a,b), vessel-ray pit membranes, the amorphous layer (Fig. 5c) and in pseudotori (Fig. 5d). The pattern described above was not found in control samples prepared without ruthenium red, indicating that osmium tetraoxide alone was not responsible for the differential contrast. The main part of intervessel pit membranes could be distinguished in samples of all species as a very faint, almost electron-transparent granular layer. No increase in electron density of the main part of intervessel pit membranes was apparent in samples stained in ruthenium red.

Calcium localization with TEM

The antimonate technique was used to localize electron dense calcium precipitate in TEM-samples. In agreement with the calcium chelating experiments described above (Fig. 2b), the precipitates often formed a thin layer of clumps along the inner vessel walls. By contrast, precipitates were less common in fiber lumens. A distinct layer of precipitate was consistently observed in the annulus region of interconduit pits (Figs 3d, 4b). This pattern matched the labeling with JIM5. The distribution of calcium precipitate also matched the JIM5 labeling patterns found in pseudotori (compare Fig. 4a,b). Precipitate was consistently found on the surface of vessel-ray pit membranes (Fig. 4d, arrows). While the distribution of calcium precipitate closely matched the distinct JIM5 labeling patterns described above, there was less agreement with JIM7 labeling. Calcium precipitate was not found throughout the entire annulus or the entire vessel-ray pit membrane. Instead, the precipitate often formed a lining around the annulus (Fig. 3d) and was restricted to the surface of vessel-ray pit membranes (Fig. 4d).

Distribution of rhamnogalacturonan I and xyloglucan

The signal for the other antibodies, LM6 and LM15, tended to be weaker and more variable than the patterns seen for JIM5 and JIM7. Nevertheless, both antibodies were localized in the cml. Weak labeling of anti-RG-I LM6 occurred in vessel-ray pit membranes. The LM6 epitope was most abundant in the amorphous layer of ray cells (Fig. S2a), where it provided a strong signal in all species. While LM6 labeled pseudotori (Fig. S2c), the LM6 signal was not enriched in annuli. Intervessel pit membranes of *P. virginiana* showed weak labeling with LM6, but this pattern could not be confirmed in the other species.

The LM15 xyloglucan epitope was consistently found in the cml (Fig. S2b) and in the outer layer of cell corners (Fig. S2d). Weak labeling was also found in intervessel pit membranes of *P. virginiana* and *A. alnifolia* (Fig. S2b, dark grey arrow). LM15 labeling was not observed in pseudotori, vessel-ray pit membranes, and in the amorphous layer (Table 1).

Table 2 Pit membrane diameter (D_m), annulus length and intensity of homogalacturonan labeling in the annulus in *Betula papyrifera*, *Populus balsamifera*, *Prunus virginiana* and *Amelanchier alnifolia*

			Number of gold particles		
Species	D_m (μm)	Annulus length (nm)	JIM5	JIM7	JIM5 : JIM7
Betula papyrifera	2.3 ± 0.03 (86)^a	141 ± 8 (24)^a	12 ± 1 (13)^a	5 ± 1 (13)^a	2.49
Populus balsamifera	6.8 ± 0.06 (85)^b	275 ± 24 (20)^b	9 ± 2 (16)^{ab}	10 ± 2 (6)^{ab}	0.82
Prunus virginiana	4.6 ± 0.05 (87)^c	331 ± 27 (20)^b	5 ± 0 (6)^b	10 ± 2 (15)^b	0.48
Amelanchier alnifolia	4.8 ± 0.05 (76)^c	351 ± 23 (20)^b	6 ± 1 (15)^b	15 ± 1 (9)^b	0.44

The intensity of the labeling was assessed by counting the number of gold particles localized in the annulus. The JIM5 : JIM7 antibody ratio is indicative of the ratio of low methyl-esterified to high methyl-esterified homogalacturonans. Values represent means ± SE, the number of individual pits and annuli used for these measurements is indicated in brackets. Different letters indicate that the means were significantly different between the species, one-way ANOVA followed by Tukey HSD test ($P < 0.05$).

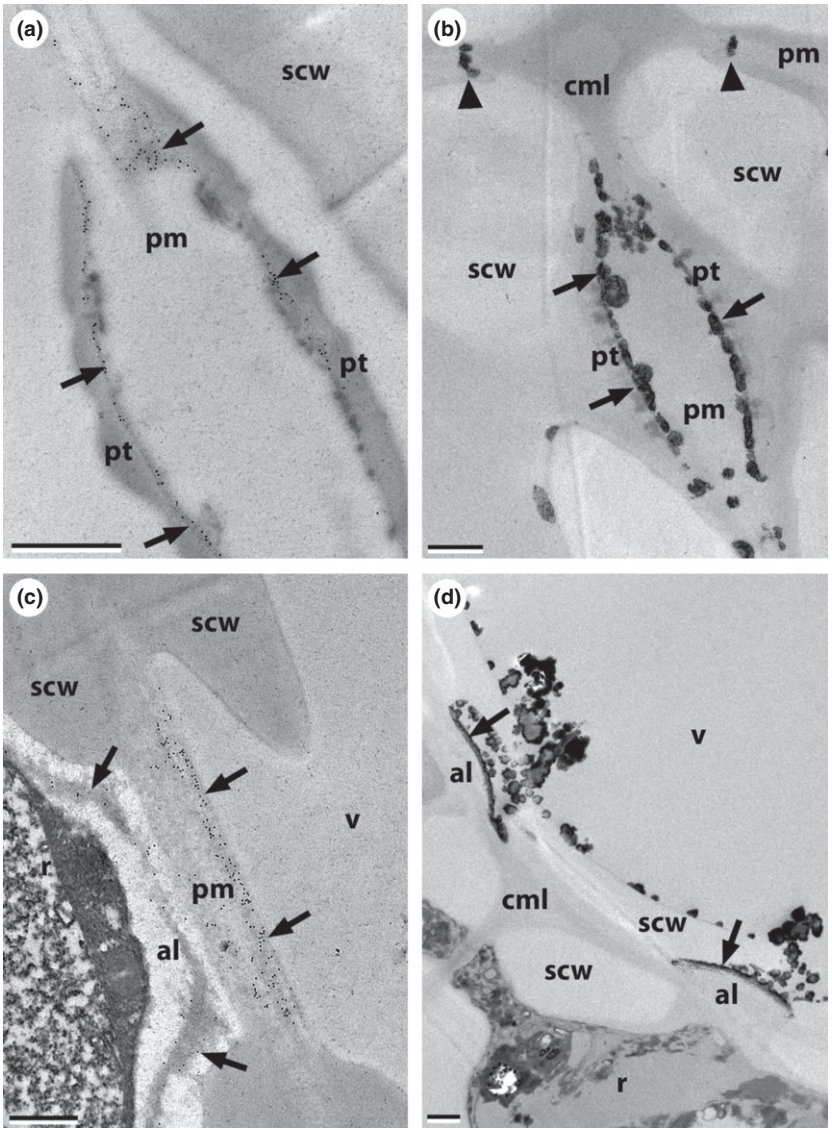

Fig. 4 Corresponding patterns of immunolabeling with JIM5 antibody (a,c) and calcium localization (b,d) in pseudotori (a, b) and vessel-ray pits (c,d) of *Amelanchier alnifolia* as observed with transmission electron microscopy. Gold particles and calcium precipitate were localized on the inner surface of pseudotori (arrows in a and b) of imperforate tracheary elements. Precipitates were also evident in the annulus (arrowheads in b). JIM5 epitopes were abundant in the vessel-ray pit membrane (pm in c) and in the amorphous layer (al) of ray cells (c). The greatest labeling density within the vessel-ray pit membrane was found close to the surface of the membrane, near the vessel lumen (v, arrows; panel c only). Correspondingly, a distinct layer of precipitates was observed lining the outer vessel-ray pit membrane surface in samples treated with antimonate (d). Precipitates were also found around the periphery of the vessel lumen. al, amorphous layer; cml, compound middle lamella; pm, pit membrane; pt, pseudotorus; r, ray cell; scw, secondary cell wall; v, vessel lumen. Bars, 0.5 μm.

Discussion

A significant increase in xylem vulnerability after perfusion with calcium chelating solution was found in three out of four species studied (Fig. 1). The magnitude of the shift was proportional to the native vulnerability of the species, with the more resistant species showing larger shifts (Fig. S1). These results are in agreement with previous findings of Herbette & Cochard (2010). In addition, our data indicate that at least some highly vulnerable species can become even more vulnerable after calcium removal, as shown by the 0.6 MPa shift seen in *P. balsamifera*. The shift in vulnerability after calcium removal was highly reproducible, suggesting that it was caused by a 'controlled' change in pit membrane properties rather than a complete loss of integrity of the pit membranes. Sperry & Tyree (1988) and Herbette & Cochard (2010) suggested that the shift in vulnerability is caused by disruptions of calcium–HG crosslinks in intervessel pit membranes that would change the rigidity and stretching properties of the membranes.

The pectin localization experiments conducted in this study showed that the main part of intervessel pit membranes in all four species contained very little or no HG. Thus, our original hypothesis that there is a link between the presence or absence of HG in the pit membrane and the magnitude of the vulnerability shift was not supported. The only portion of the membrane that was rich in HG was the marginal annulus region. The pit membrane annulus is a conspicuous feature of the pit membrane and has often been noted by wood anatomists. A distinct annulus occurs both in interconduit pits of angiosperms (Schmid, 1965; Schmid & Machado, 1968; Jansen *et al.*, 2009; Gortan *et al.*, 2011) as well as in torus–margo pits of gymnosperms

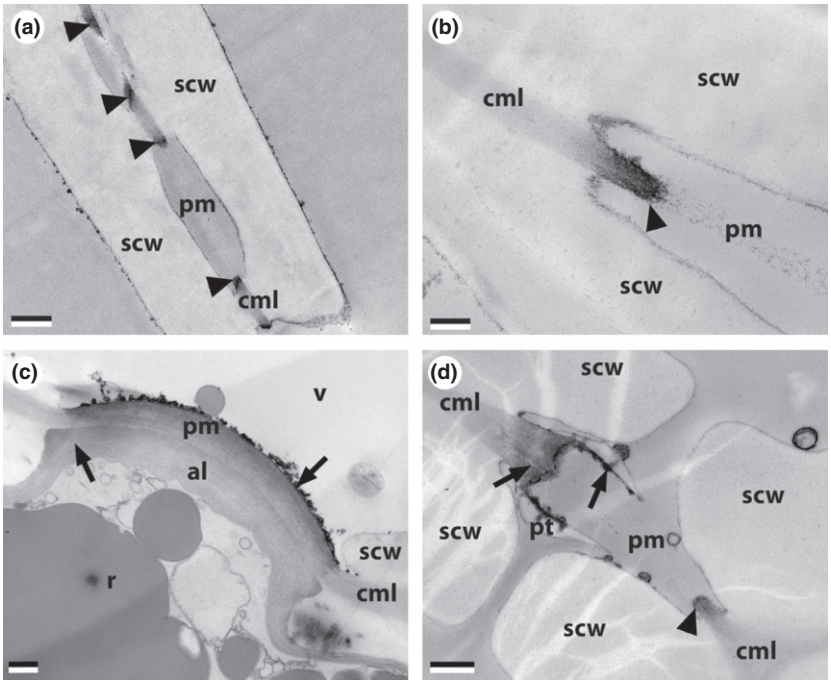

Fig. 5 Ruthenium red staining of acidic pectin in the xylem of *Betula papyrifera* (a), *Populus balsamifera* (b,c) and *Prunus virginiana* (d). Dark, electron-dense regions (arrowheads, arrows) show a positive staining reaction. Ruthenium red staining was apparent in the pit membrane annulus (arrowheads in a, b and d), in the vessel-ray pit membrane (pm), the amorphous layer (al) (arrows in c), as well as the inner surface of pseudotori (pt, arrows in d). There was a close correspondence between ruthenium red staining and JIM5 immunolabeling (compare this figure with Figs 3, 4). al, amorphous layer; cml, compound middle lamella; pm, pit membrane; pt, pseudotorus; r, ray cell; scw, secondary cell wall; v, vessel lumen. Bars, (a,c,d) 0.5 μm, (b) 0.2 μm.

(Liese, 1965; Dute *et al.*, 2008; Pittermann *et al.*, 2010). Under TEM, the annulus typically appears more electron-dense than the rest of the membrane. However, the opposite pattern has also been found in a few species (Schmitz *et al.*, 2007; Jansen *et al.*, 2009; Gortan *et al.*, 2011). To the best of our knowledge, it is not known whether the annulus plays a physiological role or if it simply relates to pit development (e.g. the enzymes that remodel the pit membrane may have restricted access to the marginal membrane region).

A high HG content in the annulus was consistently observed in all four species studied and agrees with our previous observations on hybrid poplar saplings (Plavcová *et al.*, 2011) as well as earlier reports (O'Brien, 1970). Furthermore, the anti-RG-I antibody did not display an increased labeling density in the annulus, indicating that it is specifically the HG domain of pectins that is enriched in the annulus. Homogalacturonans are known for their calcium-binding capacity (MacDougall *et al.*, 2001b; Proseus & Boyer, 2008) and this premise was confirmed by our calcium localization experiment. Hence, it is possible that the effect of calcium removal on xylem vulnerability is realized through the disruption of the HG-calcium superstructure within the annulus. The fact that the magnitude of the shift in the four species studied was proportional to the length of the annulus further supports this hypothesis.

Based on our findings, we propose that the pit membrane should not be viewed as an isotropic material. Instead, there are two chemically and structurally distinct domains (the pit membrane annulus and the main part of the membrane) that likely exhibit different mechanical properties. A growing body of evidence suggests that the large pressure difference that is exerted on the pit membrane before air seeding results in pit membrane stretching, and that the extent of membrane deflection influences the cavitation threshold. Features that minimize pit membrane deflection such as vestures (Choat *et al.*, 2004) or shallow pit chambers (Hacke & Jansen, 2009; Lens *et al.*, 2011) were found in embolism-resistant xylem. Although calcium crosslinks can substantially enhance cell wall strength (Parre & Geitmann, 2005; Cybulska *et al.*, 2011), cellulose microfibrils most likely represent the main load-bearing component of pit membranes and limit the degree of membrane deformation (Petty, 1972; Sperry & Hacke, 2004). The orientation of microfibrils is critical for mechanical properties. The wall is more pliable in the direction perpendicular to the prevailing orientation of the microfibrils. In the pit membrane, the microfibrils seem to be oriented randomly. However, it is not clear whether the same pattern of microfibril orientation is maintained in the annulus. Observations of developing pits suggest that microfibrils are deposited in a circular fashion near the pit border (Wardrop, 1954; Imamura & Harada, 1973; Chaffey *et al.*, 1997). This deposition pattern is usually interpreted as an initial step in the formation of the pit border. However, Imamura & Harada (1973) state: '…the circularly oriented microfibrils have been laid down making the periphery of the pit area, called the pit annulus'.

If microfibrils in the annulus are oriented in a circular fashion, the annulus would extend more than the rest of the membrane during air seeding as the cellulose microfibrils would move apart. When stems were perfused with the

calcium chelating agent, the annulus region may have become looser and even more extensible. Thus, it is possible that calcium removal led to the formation of small pores or micro-cracks within the annulus or the annulus-membrane interface through which air could penetrate and cause embolism. Alternatively, calcium removal from the annulus may allow for increased pit membrane deflection, which in turn would lead to a widening of membrane pores. A more extensible annulus would allow the pit membrane to deflect further and aspirate sooner against the pit border. As the membrane continues to deflect through the pit aperture, the pores will start to enlarge even more and air seeding will occur at less negative xylem pressure (Sperry & Hacke, 2004).

Betula papyrifera was the only species in this study that did not show a shift in vulnerability after calcium removal. Although HG and calcium were present in the pit membrane annulus, annuli of *B. papyrifera* were significantly shorter than those of the other three species. This may explain why the effect of calcium removal was less pronounced in *B. papyrifera*. In addition, intervessel pits of *B. papyrifera* were much smaller than those of the other species. With all other parameters being equal, smaller pits should show less membrane deflection than larger ones (see Eqn 8 in Sperry & Hacke, 2004). Membrane deflection in *B. papyrifera* may therefore be minimal. However, pit membrane diameter alone does not have a strong effect on xylem vulnerability (Jansen *et al.*, 2009; Lens *et al.*, 2011). Pit membrane thickness can also play a role. More detailed knowledge of the overall pit geometry and mechanical properties is necessary to decipher if and how pit membrane deflection influences the air seeding threshold. Our results also indicate that HG in annuli of *B. papyrifera* exhibited a relatively low degree of methyl-esterification (Table 2). Low-esterified HG binds calcium more tightly than does high methoxyl pectin (Tibbits *et al.*, 1998). It is possible that calcium was less susceptible to sequestration in *B. papyrifera* and that the annulus consequently retained its original strength. However, the data on labeling density shown in Table 2 should be interpreted with caution as they originate from only one or two independent immunolabeling experiments per species.

The proposed hypothesis that changes in the extensibility of the annulus can induce increased vulnerability is speculative. An alternative explanation would be that a low amount of HG and calcium is present in interconduit pit membranes, and that this small amount was not detected by the methods employed in this study. Following this argument, one would expect that HG and calcium were completely removed during pit development in *B. papyrifera* (which did not shift), but not in the other species, which did shift. This seems unlikely and none of our data supported this view. The different methods employed in this study all indicated that the annulus is the region of the pit membrane with the highest HG and calcium content. It seems improbable that the treatment with calcium chelating agents would not have any effect on it.

Our results highlight the differences in interconduit and vessel-ray pit membrane chemistry. In contrast to intervessel pits, the entire surface of vessel-ray pit membranes was rich in pectins (Figs 4c, 5c) and calcium (Figs 2, 4d). Vessel-ray pit membranes lacked an annulus. The transitional region between cml and pit membrane did not show enhanced HG-labeling, further supporting that the annulus might have a specific role in interconduit pit functioning. Pectins were previously found in vessel-ray pit membranes of *Prunus persica* (Wisniewski & Davis, 1995). It has been suggested that pectinaceous vessel-ray pit membranes effectively isolate intracellular water from extracellular ice, thereby conferring the ability of the tissue to undergo supercooling.

This study also provides information on pseudotori. The function, if any, of these peculiar structures is unknown. Pseudotori occur in tracheary elements of several woody taxa, including Rosaceae, Ericaceae, and Oleaceae (Jansen *et al.*, 2007; Rabaey *et al.*, 2008). Pseudotori develop as secondary thickenings following the formation of plasmodesmata-associated primary thickenings. Later in development, autolytic enzymes remove the primary thickenings leaving the pseudotori intact, and the tracheary cell undergoes programmed cell death (Rabaey *et al.*, 2008). Our immunolabeling experiments complement this description with some chemistry data. We often observed a nonhydrolysed portion of the pit membrane that was protected by pseudotorus caps. This finding further highlights the substantial remodeling and hydrolysis that affects most of the noncellulosic components during the development of interconduit pit membranes (O'Brien, 1970; Czaninski, 1972). In addition, the colocalization of HG and calcium (Fig. 4a,b) demonstrates that calcium abundantly occurs in association with HG in the xylem.

A different pattern in pectin distribution was recently found in pit membranes of four Lauraceae species (Gortan *et al.*, 2011). In these species, intervessel pit membranes reacted strongly with ruthenium red, while annuli and vessel-ray pit membranes showed a negative reaction. Pectins were also present in the pit membranes of grapevine (Sun *et al.*, 2011) and conifers (Hafren *et al.*, 2000). Thus, it is obvious that substantial variability in pit membrane chemistry exists across different plant taxa. Future research will likely highlight the functional and ecological significance of these differences in pit chemistry. A comparative study using angiosperm species with high and low pectin content in their pit membranes would provide further insights into the role of pectins in pit membrane functioning. For example, it would be helpful to see whether a similar shift in vulnerability after calcium removal occurs in Lauraceae species and whether the high pectin content in pit membranes of Lauraceae is associated with high pit resistance and with

the ability to trap solutes within refilling vessels (Hacke & Sperry, 2003; Nardini *et al.*, 2011).

In addition, the relationship between shifts in vulnerability and the ion-mediated increase in hydraulic conductivity (Zwieniecki *et al.*, 2001; Gasco *et al.*, 2006) needs to be evaluated as both phenomena are attributed to the presence of HG in the pit membranes. However, there are also distinct differences that may partly uncouple these two phenomena. For example, a broader spectrum of pectin types can be responsible for the ionic effect while only the long linear stretches of GalA that are typical for the HG domain are capable of substantial calcium crosslinking. All four species in this study showed a relatively weak ionic effect between 5% and 16% (data not shown). The magnitude of the ionic effect did not correspond with ΔP_{50}. It is not clear whether the hydrogel behavior of pectins in the annulus could influence k_h. However, it is possible that the tension of the annulus, as determined by the ionic interactions, transmits to the cellulosic matrix of the pit membrane, thereby stretching and relaxing the membrane pores.

In conclusion, this study enhances our knowledge of the chemical composition of pit membranes, which is a prerequisite for a better understanding of the role of these microvalves in xylem functioning. Our results suggest that there is no link between the general presence or absence of HG in intervessel pit membranes and the shift in vulnerability after calcium removal. We provide evidence that pectic HG are not homogeneously distributed in intervessel pit membranes. In the four species studied, the main part of the membrane contained very little or no pectins whereas the annulus showed substantial enrichment in HG-labeling. Calcium precipitation experiments confirmed that calcium colocalizes with HG in the annulus. We therefore hypothesize that the disruption of HG-calcium crosslinks within the annulus can lead to increased vulnerability to cavitation. Our results also highlight differences in chemical composition between interconduit and vessel-ray pit membranes. Observed differences in chemistry likely reflect the different biological functions of these pit types. While intervessel pits facilitate water flow, vessel-ray pits may be designed to provide a selective barrier between living ray cells and dead vessel elements.

Acknowledgements

We thank Arlene Oatway (Advanced Microscopy Unit, Department of Biological Sciences, University of Alberta, Canada), Dr Ming H. Chen (Akio Chen Enterprises, Inc., Edmonton, Canada), George Braybrook, and De-Ann Rollings (Scanning Electron Microscope Facility, Department of Earth and Atmospheric Sciences, University of Alberta, Canada) for their help with electron microscopy. We thank Prof. J.P. Knox for the kind gift of JIM5 and JIM7 antibodies. Funding (to UH) was provided by an Alberta Ingenuity New Faculty Award and an NSERC Discovery grant. UH also acknowledges support from the Canada Research Chair Program and the Canada Foundation for Innovation.

References

Alder NN, Pockman WT, Sperry JS, Nuismer S. 1997. Use of centrifugal force in the study of xylem cavitation. *Journal of Experimental Botany* **48**: 665–674.

Baier M, Goldberg R, Catesson A-M, Liberman M, Bouchemal N, Michon V, Penhoat CH. 1994. Pectin changes in samples containing poplar cambium and inner bark in relation to the seasonal cycle. *Planta* **193**: 446–454.

Boyce CK, Zwieniecki MA, Cody GD, Jacobsen C, Wirick S, Knoll AH, Holbrook NM. 2004. Evolution of xylem lignification and hydrogel transport regulation. *Proceedings of the National Academy of Sciences, USA* **101**: 17555–17558.

Braun HJ. 1970. *Funktionelle Histologie der sekundären Sprossachse. I. Das Holz*. Berlin: Gebrüder Borntraeger.

Brodersen CR, McElrone AJ, Choat B, Matthews MA, Shackel KA. 2010. The dynamics of embolism repair in xylem: *in vivo* visualizations using high-resolution computed tomography. *Plant Physiology* **154**: 1088–1095.

Caffall KH, Mohnen D. 2009. The structure, function, and biosynthesis of plant cell wall pectic polysaccharides. *Carbohydrate Research* **344**: 1879–1900.

Carlquist S. 1986. Terminology of imperforate tracheary elements – a reply. *Iawa Bulletin* **7**: 168–170.

Cassab GI. 1998. Plant cell wall proteins. *Annual Review of Plant Physiology and Plant Molecular Biology* **49**: 281–309.

Chaffey NJ. 2002. Conventional (chemical-fixation) transmission electron microscopy and cytochemistry of angiosperm trees. In: Chaffey NJ, ed. *Wood formation in trees: cell and molecular biology techniques*. London, UK: Taylor & Francis, 41–64.

Chaffey NJ, Barnett JR, Barlow PW. 1997. Cortical microtubule involvement in bordered pit formation in secondary xylem vessel elements of *Aesculus hippocastanum* L. (Hippocastanaceae): a correlative study using electron microscopy and indirect immunofluorescence microscopy. *Protoplasma* **197**: 64–75.

Choat B, Cobb AR, Jansen S. 2008. Structure and function of bordered pits: new discoveries and impacts on whole-plant hydraulic function. *New Phytologist* **177**: 608–625.

Choat B, Jansen S, Zwieniecki MA, Smets E, Holbrook NM. 2004. Changes in pit membrane porosity due to deflection and stretching: the role of vestured pits. *Journal of Experimental Botany* **55**: 1569–1575.

Cochard H, Herbette S, Hernandez E, Holtta T, Mencuccini M. 2010. The effects of sap ionic composition on xylem vulnerability to cavitation. *Journal of Experimental Botany* **61**: 275–285.

Cybulska J, Zdunek A, Konstankiewicz K. 2011. Calcium effect on mechanical properties of model cell walls and apple tissue. *Journal of Food Engineering* **102**: 217–223.

Czaninski Y. 1972. Ultrastructural observations on hydrolysis of primary walls of vessels in *Robinia pseudo-acacia* L. and *Acer pseudoplatanus* L. *Comptes Rendus Hebdomadaires Des Seances De L Academie Des Sciences Serie D* **275**: 361–363.

De Boer AH, Volkov V. 2003. Logistics of water and salt transport through the plant: structure and functioning of the xylem. *Plant, Cell & Environment* **26**: 87–101.

Dute R, Hagler L, Black A. 2008. Comparative development of intertracheary pit membranes in *Abies firma* and *Metasequoia glyptostroboides*. *IAWA Journal* **29**: 277–289.

Ermel FF, Follet-Gueye ML, Cibert C, Vian B, Morvan C, Catesson AM, Goldberg R. 2000. Differential localization of arabinan and galactan

side chains of rhamnogalacturonan I in cambial derivatives. *Planta* **210**: 732–740.

Evert RF. 2006. *Esau's plant anatomy: meristems, cells, and tissues of the plant body: their structure, function, and development*. Hoboken, NJ, USA: John Wiley & Sons, Inc.

Funada R, Catesson AM. 1991. Partial cell wall lysis and the resumption of meristematic activity in *Fraxinus excelsior* cambium. *Iawa Bulletin* **12**: 439–444.

Gasco A, Nardini A, Gortan E, Salleo S. 2006. Ion-mediated increase in the hydraulic conductivity of Laurel stems: role of pits and consequences for the impact of cavitation on water transport. *Plant, Cell & Environment* **29**: 1946–1955.

Gortan E, Nardini A, Salleo S, Jansen S. 2011. Pit membrane chemistry influences the magnitude of ion-mediated enhancement of xylem hydraulic conductance in four Lauraceae species. *Tree Physiology* **31**: 48–58.

Guglielmino N, Liberman M, Jauneau A, Vian B, Catesson AM, Goldberg R. 1997. Pectin immunolocalization and calcium visualization in differentiating derivatives from poplar cambium. *Protoplasma* **199**: 151–160.

Guillemin F, Guillon F, Bonnin E, Devaux MF, Chevalier T, Knox JP, Liners F, Thibault JF. 2005. Distribution of pectic epitopes in cell walls of the sugar beet root. *Planta* **222**: 355–371.

Hacke UG, Jansen S. 2009. Embolism resistance of three boreal conifer species varies with pit structure. *New Phytologist* **182**: 675–686.

Hacke UG, Sperry JS. 2003. Limits to xylem refilling under negative pressure in *Laurus nobilis* and *Acer negundo*. *Plant, Cell & Environment* **26**: 303–311.

Hacke UG, Sperry JS, Wheeler JK, Castro L. 2006. Scaling of angiosperm xylem structure with safety and efficiency. *Tree Physiology* **26**: 689–701.

Hafren J, Daniel G, Westermark U. 2000. The distribution of acidic and esterified pectin in cambium, developing xylem and mature xylem of *Pinus sylvestris*. *IAWA Journal* **21**: 157–168.

Harrak H, Chamberland H, Plante M, Bellemare C, Lafontaine JG, Tabaeizadeh Z. 1999. A proline-, threonine-, and glycine-rich protein down-regulated by drought is localized in the cell wall of xylem elements. *Plant Physiology* **121**: 557–564.

Herbette S, Cochard H. 2010. Calcium is a major determinant of xylem vulnerability to cavitation. *Plant Physiology* **153**: 1932–1939.

van Ieperen W. 2007. Ion-mediated changes of xylem hydraulic resistance in planta: fact or fiction? *Trends in Plant Science* **12**: 137–142.

Imamura Y, Harada H. 1973. Electron-microscopic study on development of bordered pit in coniferous tracheids. *Wood Science and Technology* **7**: 189–205.

Jansen S, Choat B, Pletsers A. 2009. Morphological variation of intervessel pit membranes and implications to xylem function in angiosperms. *American Journal of Botany* **96**: 409–419.

Jansen S, Gortan E, Lens F, Lo Gullo MA, Salleo S, Scholz A, Stein A, Trifilo P, Nardini A. 2011. Do quantitative vessel and pit characters account for ion-mediated changes in the hydraulic conductance of angiosperm xylem? *New Phytologist* **189**: 218–228.

Jansen S, Sano Y, Choat B, Rabaey D, Lens F, Dute RR. 2007. Pit membranes in tracheary elements of Rosaceae and related families: new records of tori and pseudotori. *American Journal of Botany* **94**: 503–514.

Jarbeau JA, Ewers FW, Davis SD. 1995. The mechanism of water-stress-induced embolism in two species of chaparral shrubs. *Plant, Cell & Environment* **18**: 189–196.

Knox JP, Linstead PJ, King J, Cooper C, Roberts K. 1990. Pectin esterification is spatially regulated both within cell walls and between developing tissues of root apices. *Planta* **181**: 512–521.

Lens F, Sperry JS, Christman MA, Choat B, Rabaey D, Jansen S. 2011. Testing hypotheses that link wood anatomy to cavitation resistance and hydraulic conductivity in the genus *Acer*. *New Phytologist* **190**: 709–723.

Li YY, Sperry JS, Taneda H, Bush SE, Hacke UG. 2008. Evaluation of centrifugal methods for measuring xylem cavitation in conifers, diffuse- and ring-porous angiosperms. *New Phytologist* **177**: 558–568.

Liese W. 1965. The fine structure of bordered pits in softwoods. In: Cote WA, ed. *Cellular ultrastructure of woody plants*. Syracuse, NY, USA: Syracuse University Press, 271–290.

Lopez-Portillo J, Ewers FW, Angeles G. 2005. Sap salinity effects on xylem conductivity in two mangrove species. *Plant, Cell & Environment* **28**: 1285–1292.

MacDougall AJ, Brett GM, Morris VJ, Rigby NM, Ridout MJ, Ring SG. 2001a. The effect of peptide–pectin interactions on the gelation behaviour of a plant cell wall pectin. *Carbohydrate Research* **335**: 115–126.

MacDougall AJ, Rigby NM, Ryden P, Tibbits CW, Ring SG. 2001b. Swelling behavior of the tomato cell wall network. *Biomacromolecules* **2**: 450–455.

Marcus SE, Verhertbruggen Y, Herve C, Ordaz-Ortiz JJ, Farkas V, Pedersen HL, Willats WGT, Knox JP. 2008. Pectic homogalacturonan masks abundant sets of xyloglucan epitopes in plant cell walls. *BMC Plant Biology* **8**: 60.

Micheli F. 2001. Pectin methylesterases: cell wall enzymes with important roles in plant physiology. *Trends in Plant Science* **6**: 414–419.

Micheli F, Ermel FF, Bordenave M, Richard L, Goldberg R. 2002. Cell walls of woody tissues: cytochemical, biochemical and molecular analysis of pectins and pectin methylesterases. In: Chaffey NJ, ed. *Wood formation in trees: cell and molecular biology techniques*. London, UK: Taylor & Francis, 179–200.

Morrow AC, Dute RR. 1998. Development and structure of pit membranes in the rhizome of the woody fern *Botrychium dissectum*. *IAWA Journal* **19**: 429–441.

Nardini A, Grego F, Trifilo P, Salleo S. 2010. Changes of xylem sap ionic content and stem hydraulics in response to irradiance in *Laurus nobilis*. *Tree Physiology* **30**: 628–635.

Nardini A, Lo Gullo MA, Salleo S. 2011. Refilling embolized xylem conduits: is it a matter of phloem unloading? *Plant Science* **180**: 604–611.

O'Brien TP. 1970. Further observations on hydrolysis of the cell wall in the xylem. *Protoplasma* **69**: 1–14.

O'Neill MA, William SY. 2003. The composition and structure of plant primary walls. In: Rose JKC, ed. *The plant cell wall, annual plant reviews*. Oxford, UK: Blackwell Publishing Ltd, 1–54.

Parre E, Geitmann A. 2005. Pectin and the role of the physical properties of the cell wall in pollen tube growth of *Solanum chacoense*. *Planta* **220**: 582–592.

Petty JA. 1972. Aspiration of bordered pits in conifer wood. *Proceedings of the Royal Society of London Series B-Biological Sciences* **181**: 395–406.

Pittermann J, Choat B, Jansen S, Stuart SA, Lynn L, Dawson TE. 2010. The relationships between xylem safety and hydraulic efficiency in the Cupressaceae: the evolution of pit membrane form and function. *Plant Physiology* **153**: 1919–1931.

Pittermann J, Sperry JS, Hacke UG, Wheeler JK, Sikkema EH. 2005. Torus–margo pits help conifers compete with angiosperms. *Science* **310**: 1924.

Plavcová L, Hacke UG, Sperry JS. 2011. Linking irradiance-induced changes in pit membrane ultrastructure with xylem vulnerability to cavitation. *Plant, Cell & Environment* **34**: 501–513.

Proseus TE, Boyer JS. 2008. Calcium pectate chemistry causes growth to be stored in *Chara corallina*: a test of the pectate cycle. *Plant, Cell & Environment* **31**: 1147–1155.

R Development Core Team. 2009. *R: A language and environment for statistical computing*. Vienna, Austria: R Foundation for Statistical Computing. http://www.R-project.org.

Rabaey D, Lens F, Huysmans S, Smets E, Jansen S. 2008. A comparative ultrastructural study of pit membranes with plasmodesmata associated thickenings in four angiosperm species. *Protoplasma* **233**: 255–262.

Reynolds ES. 1963. The use of lead citrate at high pH as an electron opaque stain in electron microscopy. *Journal of Cell Biology* **17**: 208–212.

Ryden P, MacDougall AJ, Tibbits CW, Ring SG. 2000. Hydration of pectic polysaccharides. *Biopolymers* **54**: 398–405.

Salleo S, Trifilo P, Esposito S, Nardini A, Lo Gullo MA. 2009. Starch-to-sugar conversion in wood parenchyma of field-growing *Laurus nobilis* plants: a component of the signal pathway for embolism repair? *Functional Plant Biology* **36**: 815–825.

Sauter JJ, Iten W, Zimmermann MH. 1973. Studies on the release of sugars into the vessels of sugar maple (*Acer saccharum* Marsh.). *Canadian Journal of Botany–Revue Canadienne De Botanique* **51**: 1–8.

Sauter JJ, Van Cleve B. 1992. Seasonal variation of amino acids in the xylem sap of "*Populus* × *canadensis*" and its relation to protein body mobilization. *Trees – Structure and Function* **7**: 26–32.

Schmid R. 1965. The fine structure of pits in hardwoods. In: Cote WA, ed. *Cellular ultrastructure of woody plants*. Syracuse, NY, USA: Syracuse University Press, 291–304.

Schmid R, Machado RD. 1968. Pit membranes in hardwoods – fine structure and development. *Protoplasma* **66**: 185–204.

Schmitz N, Jansen S, Verheyden A, Kairo JG, Beeckman H, Koedam N. 2007. Comparative anatomy of intervessel pits in two mangrove species growing along a natural salinity gradient in Gazi Bay, Kenya. *Annals of Botany* **100**: 271–281.

Slocum RD, Roux SJ. 1982. An improved method for the sub-cellular localization of calcium using a modification of the anitmonate precipitation technique. *Journal of Histochemistry & Cytochemistry* **30**: 617–629.

Sperry JS, Hacke UG. 2004. Analysis of circular bordered pit function – I. Angiosperm vessels with homogenous pit membranes. *American Journal of Botany* **91**: 369–385.

Sperry JS, Saliendra NZ, Pockman WT, Cochard H, Cruiziat P, Davis SD, Ewers FW, Tyree MT. 1996. New evidence for large negative xylem pressures and their measurement by the pressure chamber method. *Plant, Cell & Environment* **19**: 427–436.

Sperry JS, Tyree MT. 1988. Mechanism of water stress-induced xylem embolism. *Plant Physiology* **88**: 581–587.

Sun QA, Greve LC, Labavitch JM. 2011. Polysaccharide compositions of intervessel pit membranes contribute to Pierce's disease resistance of grapevines. *Plant Physiology* **155**: 1976–1987.

Tibbits CW, MacDougall AJ, Ring SG. 1998. Calcium binding and swelling behaviour of a high methoxyl pectin gel. *Carbohydrate Research* **310**: 101–107.

Tyree MT, Zimmermann MH. 2002. *Xylem structure and the ascent of sap*. Berlin, Germany: Springer Verlag.

Valentin R, Cerclier C, Geneix N, Aguie-Beghin V, Gaillard C, Ralet MC, Cathala B. 2010. Elaboration of extensin–pectin thin film model of primary plant cell wall. *Langmuir* **26**: 9891–9898.

Wardrop AB. 1954. The mechanism of surface growth involved in the differentiation of fibres and tracheids. *Australian Journal of Botany* **2**: 165–175.

Wick SM, Hepler PK. 1980. Localization of Ca^{++}-containing antimonate precipitates during mitosis. *Journal of Cell Biology* **86**: 500–513.

Willats WGT, McCartney L, Mackie W, Knox JP. 2001. Pectin: cell biology and prospects for functional analysis. *Plant Molecular Biology* **47**: 9–27.

Wisniewski M, Davis G. 1995. Immunogold localization of pectins and glycoproteins in tissue of peach with reference to deep supercooling. *Trees* **9**: 253–260.

Wisniewski M, Davis G, Arora R. 1991. Effect of macerase, oxalic acid, and EGTA on deep supercooling and pit membrane structure of xylem parenchyma of peach. *Plant Physiology* **96**: 1354–1359.

Zwieniecki MA, Melcher PJ, Holbrook NM. 2001. Hydrogel control of xylem hydraulic resistance in plants. *Science* **291**: 1059–1062.

Supporting Information

Additional Supporting Information may be found in the online version of this article:

Fig. S1 Relationship between vulnerability to cavitation and the magnitude of vulnerability shift in four angiosperm species.

Fig. S2 Immunogold labeling of cell walls with anti-RG-I antibody LM6 and anti-xyloglucan antibody LM15.

Please note: Wiley-Blackwell are not responsible for the content or functionality of any supporting information supplied by the authors. Any queries (other than missing material) should be directed to the *New Phytologist* Central Office.